VOLUME 333 ISSUE 6
17 MARCH 2014
ISSN 0022-460X

JOURNAL OF SOUND AND VIBRATION

Available online at www.sciencedirect.com

ScienceDirect

Efficient model order reduction for dynamic systems with local nonlinearities

CrossMark

Mohsen Mohammadali *, Hamid Ahmadian

Center of Excellence in Experimental Solid Mechanics and Dynamics, School of Mechanical Engineering, Iran University of Science and Technology, Narmak, Tehran 16844, Iran

ARTICLE INFO

ABSTRACT

In the nonlinear structural analysis, the nonlinear effects are commonly localized and the rest of the structure behaves in a linear manner. Considering this fact, this research work proposes a harmonic balance solution in order to determine the nonlinear response of the structures. The solution is simplified by using an exact dynamic reduction along with the modal expansion technique. This novel approach, which is applicable to both discrete and continuous systems, converts the system equations of motion in each harmonic to a small set of nonlinear algebraic equations. The full set of system equations is reduced to a discrete system with a few generalized degrees of freedom (DOFs) confined to the localized nonlinear regions. The resultant reduced order model is shown to be accurate enough for determining the periodic response. To demonstrate the capability of the proposed method, numerical case studies for continuous and discrete systems, including systems with internal resonance, have been studied and the outcomes are validated with benchmark studies. In addition, the method is applied in the identification process of an experimental test setup with unknown frictional support parameters, and the results are presented and discussed.

1. Introduction

In many assembled structures with local nonlinearities, except for the local regions with nonlinear effects, most parts of the structures are assumed to behave linearly. Typical engineering examples of these localized nonlinearities in the mechanical systems are friction and vibro-impact in joint interfaces, local buckling, cracks, nonlinear vibration isolator, dead zone (gap) and squeeze film dampers. Consequently, the behavior of these systems is regarded as nonlinear.

Dynamic models of these structures are employed to estimate the nonlinear responses for detailed studies in various applications such as identification of unknown structural parameters or health monitoring of the structures. Usually, the dynamic properties of the structures' components are known (from analysis or measurements) as separate ingredients, and are used in the development of the assembled system models. Most nonlinear effects are confined to the interfaces between these components, and much time and effort are spent in the development of models that accurately estimate the response in the presence of these nonlinear effects.

---

* Corresponding author.
  E-mail addresses: mohammadali@iust.ac.ir, m.mohammadali@gmail.com (M. Mohammadali), ahmadian@iust.ac.ir (H. Ahmadian).

Any nonlinear response analysis involves significant computational efforts, especially when the full set of the dynamic model equations is used for the response predictions. The computational efforts increase even further, when the nonlinear model parameters are related to temperature, preload, deflection, etc.

There is a significant motivation to develop new techniques in the model order reduction (MOR) to project the nonlinear model to a condensed space and reduce the computational cost considerably. However, there are other issues such as the accuracy of these MOR techniques and selection of a suitable solution algorithm that must be considered in order to obtain an accurate prediction of the system nonlinear response.

Linear reduction techniques such as Guyan reduction, improved reduced system (IRS), iterated improved reduced system (IIRS), system equivalent reduction expansion process (SEREP) and component mode synthesis (CMS) are applied to reduce nonlinear discrete models. Ref. [1] provides details of these techniques.

Other reduction methods applied to the continuous and discrete models commonly use linear normal modes (LNMs) of the linearized systems or nonlinear normal modes (NNMs). Generation of NNMs for a small system requires significant effort [2,3], especially in the presence of internal resonances [4] and/or external excitations [5]. In large systems, one may use other reduction techniques and then generate the NNMs of the reduced model [6].

The reduction methods based on the linear MOR techniques lead to acceptable answers for weakly nonlinear systems, and by increasing the nonlinearity their accuracy is reduced due to their inaccurate approximations. In local equivalent linear stiffness method (LELSM) [7] the equivalent linear model of a nonlinear system is iteratively calculated with high computational cost, and the mode shapes of the resultant linear model are used for condensation of the nonlinear system in each step.

Choosing an appropriate solution algorithm is another aspect of nonlinear system studies. The harmonic balance method (HBM) predicts the steady-state periodic solution of structures with various types of nonlinearities. The HBM is applied to nonlinear problems such as forced excited, strongly nonlinear response, chaotic behavior, and internal resonance. In addition, the HBM is frequently used for identification and health monitoring of nonlinear systems. Furthermore, this technique is employed to estimate NNMs of nonlinear systems [2].

The HBM expands periodic response of a nonlinear system as truncated Fourier series, whose coefficients are determined by solving a set of nonlinear algebraic equations. Typically, the solution accuracy is improved by using higher-order Fourier series expansions. However, in many cases, a solution of one-term harmonic balance has adequate correlation with observed experimental data [8].

Generally, the amplitudes of higher terms in Fourier series expansions are small, and are not clearly observed in measured experimental data due to noise contamination. Therefore, one may ignore the higher terms in the identification process and expand the solution using only the lower dominant harmonics.

The harmonic balance concept is further developed to address various needs of a large class of problems. Incremental harmonic balance (IHB) [9] suggests a new method based on the HBM to determine the frequency responses of nonlinear systems. With the aim of reducing the computational cost and preserving the accuracy, adaptive HBMs (AHBMs) [10] propose selection algorithms for the order of the Fourier series expansion.

An exact reduction technique in conjunction with the HBM was proposed by Kim and Noah [11,12] for the discrete nonlinear systems. The method condenses the size of the problem into the DOFs directly subject to the nonlinear restoring forces; henceforth, these DOFs are called nonlinear DOFs. The size of the reduced model depends on the number of DOFs considered in the modeling of the localized nonlinearity. Therefore, the accuracy of the obtained results is very sensitive to the number of the nonlinear DOFs, especially when the deformed state of the nonlinear region changes significantly.

To resolve this drawback, the present study suggests expanding the nonlinear DOFs response by a few base functions. The base functions are eigenfunctions of the condensed system at each harmonic. Equally, the method extends to continuous systems of the same conditions.

The organization of this paper is as follows. In Section 2, a brief description of the method given in [11,12] is presented, and is further developed by a modal expansion technique. The method is extended for continuous systems as well. To demonstrate the capabilities of the suggested method, results of continuous and discrete case studies with/without internal resonance are compared to numerical and harmonic balance results in Section 3. Furthermore, in this section, the proposed method is employed for identification of an actual nonlinear system where the response is obtained from an experimental test setup. The parameters of nonlinear effects in the model are identified by minimizing the difference between the predicted and observed responses. Finally, Section 4 draws the conclusions.

2. Model reduction of dynamic systems with local nonlinearities

A general discrete dynamic system with localized nonlinearities is considered here, and the proposed procedure for its reduction is described. Subsequently, the technique is extended to continuous dynamic systems with localized nonlinearities.

2.1. Model reduction of discrete systems

The general form of the nonlinear discrete system is

$$\mathbf{M}\ddot{\boldsymbol{q}} + \mathbf{C}\dot{\boldsymbol{q}} + \mathbf{K}\boldsymbol{q} + \boldsymbol{f}_{nl} = \boldsymbol{f}_E, \tag{1}$$

where $\boldsymbol{q}$ is the field deformation vector, $\mathbf{M}$, $\mathbf{C}$ and $\mathbf{K}$ are mass, damping and stiffness matrices, respectively, $\boldsymbol{f}_{nl}$ is the nonlinear restoring force and $\boldsymbol{f}_E$ is the periodic excitation force. The vectors $\boldsymbol{q}, \boldsymbol{f}_{nl}$ and $\boldsymbol{f}_E$ are functions of time but the time argument, t, is dropped for convenience. The steady-state solution of Eq. (1) with the period of $T = 2\pi/\omega$ is expanded in the following form:

$$\boldsymbol{q} = \sum_{j=0}^{n} (\boldsymbol{\psi}_j \, \cos(\omega_j t) + \boldsymbol{\varphi}_j \, \sin(\omega_j t)), \tag{2}$$

where n is the truncation order, $\boldsymbol{\psi}_j$ and $\boldsymbol{\varphi}_j$ are vectors of the vibration amplitude at the frequency $\omega_j = j\omega$. Substituting Eq. (2) into Eq. (1) and employing Galerkin weighted residual method, the equations of motion weighted by the corresponding sine or cosine functions are integrated over time and are decoupled as

$$-\omega_j^2 \mathbf{M}\boldsymbol{\psi}_j + \omega_j \mathbf{C}\boldsymbol{\varphi}_j + \mathbf{K}\boldsymbol{\psi}_j + \boldsymbol{f}_{nl_{c_j}} = \boldsymbol{f}_{E_{c_j}},$$

$$-\omega_j^2 \mathbf{M}\boldsymbol{\varphi}_j - \omega_j \mathbf{C}\boldsymbol{\psi}_j + \mathbf{K}\boldsymbol{\varphi}_j + \boldsymbol{f}_{nl_{s_j}} = \boldsymbol{f}_{E_{s_j}}, \tag{3}$$

where

$$\{\boldsymbol{f}_{X_{c_j}}, \boldsymbol{f}_{X_{s_j}}\} = (1 + \text{sgn}(j)) \frac{\omega}{2\pi} \int_0^{2\pi/\omega} \{\boldsymbol{f}_X \, \cos(\omega_j t), \boldsymbol{f}_X \, \sin(\omega_j t)\} \mathrm{d}t \quad X = nl, E.$$

Eq. (3) expresses one static equilibrium condition ($j = 0$) and $2n$ dynamic equations ($j = 1, 2, \ldots, n$). Employing the unit imaginary, $\iota = \sqrt{-1}$, Eq. (3) is rewritten in a complex form as

$$(-\omega_j^2 \mathbf{M} - \iota\omega_j \mathbf{C} + \mathbf{K})\boldsymbol{\chi}_j + \boldsymbol{f}_{nl_j} = \boldsymbol{f}_{E_j}, \tag{4}$$

where

$$\boldsymbol{\chi}_j = \boldsymbol{\psi}_j + \iota\boldsymbol{\varphi}_j,$$

$$\boldsymbol{f}_{X_j} = \boldsymbol{f}_{X_{c_j}} + \iota\boldsymbol{f}_{X_{s_j}} \quad X = nl, E.$$

In the case of localized nonlinearities, it is possible to write the nonlinear force vector in the following form:

$$\boldsymbol{f}_{nl} = \left\{ \begin{array}{c} \boldsymbol{f}_{nl_\alpha} \\ \boldsymbol{0} \end{array} \right\}. \tag{5}$$

Furthermore, the deformation field is divided into two vectors with subscripts α and β, which stand for active or master coordinates and deleted or slave coordinates, respectively. The master coordinates experience nonlinear restoring forces, and linear restoring forces drive the slave coordinates. Furthermore, vector $\boldsymbol{f}_E$, and matrices $\mathbf{M}$, $\mathbf{C}$ and $\mathbf{K}$ are partitioned appropriately with respect to master and slave coordinates with subscripts α and β. Subsequently, the equations of motion (4) are rearranged as

$$\left(-\omega_j^2 \begin{bmatrix} \mathbf{M}_{\alpha\alpha} & \mathbf{M}_{\alpha\beta} \\ \mathbf{M}_{\beta\alpha} & \mathbf{M}_{\beta\beta} \end{bmatrix} - \iota\omega_j \begin{bmatrix} \mathbf{C}_{\alpha\alpha} & \mathbf{C}_{\alpha\beta} \\ \mathbf{C}_{\beta\alpha} & \mathbf{C}_{\beta\beta} \end{bmatrix} + \begin{bmatrix} \mathbf{K}_{\alpha\alpha} & \mathbf{K}_{\alpha\beta} \\ \mathbf{K}_{\beta\alpha} & \mathbf{K}_{\beta\beta} \end{bmatrix} \right) \left\{ \begin{array}{c} \boldsymbol{\chi}_{\alpha_j} \\ \boldsymbol{\chi}_{\beta_j} \end{array} \right\} + \left\{ \begin{array}{c} \boldsymbol{f}_{nl_\alpha} \\ \boldsymbol{0} \end{array} \right\} = \left\{ \begin{array}{c} \boldsymbol{f}_{E_\alpha} \\ \boldsymbol{f}_{E_\beta} \end{array} \right\}. \tag{6}$$

One can eliminate $\boldsymbol{\chi}_{j_\beta}$ in Eq. (6) from the first row using the second row, this results in the exact reduced form of equations of motion

$$(-\omega_j^2 \mathbf{M}_{\alpha\alpha} - \iota\omega_j \mathbf{C}_{\alpha\alpha} + \mathbf{K}_{\alpha\alpha} - \mathbf{K}_{M_j})\boldsymbol{\chi}_{\alpha_j} + \boldsymbol{f}_{nl_{\alpha j}} = \boldsymbol{f}_{E_{\alpha j}} - \boldsymbol{f}_{ET_{\beta j}}, \tag{7}$$

where

$$\mathbf{K}_{M_j} = \boldsymbol{A}_j(-\omega_j^2 \mathbf{M}_{\beta\alpha} - \iota\omega_j \mathbf{C}_{\beta\alpha} + \mathbf{K}_{\beta\alpha}),$$

$$\boldsymbol{f}_{ET_{\beta_j}} = \boldsymbol{A}_j \boldsymbol{f}_{E_{\beta_j}},$$

$$\boldsymbol{A}_j = (-\omega_j^2 \mathbf{M}_{\alpha\beta} - \iota\omega_j \mathbf{C}_{\alpha\beta} + \mathbf{K}_{\alpha\beta})(-\omega_j^2 \mathbf{M}_{\beta\beta} - \iota\omega_j \mathbf{C}_{\beta\beta} + \mathbf{K}_{\beta\beta})^{-1}.$$

The deformation field vector, $\boldsymbol{\chi}_{\alpha_j}$, can be expanded with a set of suitable base functions as described in the following. An orthogonal basis that consists of arranged vectors with minimum energy required to excite is an appropriate basis to approximate the deformation field vectors and reduce the size of the condensed system. To find such a delicate basis, $\mathbf{K}_{M_j}$ is evaluated at the frequency ω_j and is considered as a constant stiffness matrix. This leads to a linearized eigenvalue problem of

$$(-\lambda_{jk}^2 \mathbf{M}_{\alpha\alpha} - \iota\lambda_{jk} \mathbf{C}_{\alpha\alpha} + \mathbf{K}_{\alpha\alpha} - \mathbf{K}_{M_j})\boldsymbol{\phi}_{jk} = \boldsymbol{0}, \tag{8}$$

where $\boldsymbol{\phi}_{jk}$ is the kth right eigenvector and λ_{jk} is its companion eigenvalue. The vectors $\boldsymbol{\phi}_{jk}$ form an orthogonal basis for $\boldsymbol{\chi}_{\alpha_j}$ and by increasing the index k, the required energy to excite $\boldsymbol{\phi}_{jk}$ grows in the linearized condensed system. The deformation

field χ_{α_j} is expanded using a few modes of orthogonal basis ϕ_{jk} as

$$\chi_{\alpha_j} \cong \Phi_j(\eta_{c_j} + \imath\eta_{s_j}), \tag{9}$$

where η_{c_j} and η_{s_j} are unknown real vectors and Φ_j is the modal matrix in which mode shapes, ϕ_{jk}, are arranged in column fashion. Substituting Eq. (9) in Eq. (7) and using Galerkin weighted residual method, the equations of motion are transformed into

$$\Theta_j(\eta_{c_j} + \imath\eta_{s_j}) + \langle \boldsymbol{f}_{nl_{\alpha_j}}, \Phi_j \rangle = \langle \boldsymbol{f}_{E_\alpha j} - \boldsymbol{f}_{ET_{\beta_j}}, \Phi_j \rangle, \tag{10}$$

where

$$\Theta_j = \langle (-\omega_j^2 \mathbf{M}_{\alpha\alpha} - \imath\omega_j \mathbf{C}_{\alpha\alpha} + \mathbf{K}_{\alpha\alpha} - \mathbf{K}_{M_j})\Phi_j, \Phi_j \rangle,$$

and $\langle , \rangle$ is the inner product operator. The real and imaginary parts of Eq. (10) produce two different sets of nonlinear equations, and are written in the matrix form as

$$\begin{bmatrix} \mathrm{Re}(\Theta_j) & -\mathrm{Im}(\Theta_j) \\ \mathrm{Im}(\Theta_j) & \mathrm{Re}(\Theta_j) \end{bmatrix} \begin{Bmatrix} \eta_{c_j} \\ \eta_{s_j} \end{Bmatrix} + \begin{Bmatrix} \mathrm{Re}(\langle \boldsymbol{f}_{nl_{\alpha_j}}, \Phi_j \rangle) \\ \mathrm{Im}(\langle \boldsymbol{f}_{nl_{\alpha_j}}, \Phi_j \rangle) \end{Bmatrix} = \begin{Bmatrix} \mathrm{Re}(\langle \boldsymbol{f}_{E_{\alpha_j}} - \boldsymbol{f}_{ET_{\beta_j}}, \Phi_j \rangle) \\ \mathrm{Im}(\langle \boldsymbol{f}_{E_{\alpha_j}} - \boldsymbol{f}_{ET_{\beta_j}}, \Phi_j \rangle) \end{Bmatrix}. \tag{11}$$

The periodic solution of equations of motion is obtained by solving the above nonlinear algebraic equations.

2.2. Reduction of continuous systems

The general form of the equations of motion for the continuous system is

$$\mathbf{M}\ddot{\boldsymbol{q}} + \mathbf{C}\dot{\boldsymbol{q}} + \mathbf{K}\boldsymbol{q} + \boldsymbol{f}_{nl} = \boldsymbol{f}_E,$$
$$\mathbf{L}\boldsymbol{q} = \mathbf{0} \quad \boldsymbol{x} \in \boldsymbol{x}_B. \tag{12}$$

where $\boldsymbol{q}$ is the field deformation vector, $\mathbf{K}$, $\mathbf{M}$ and $\mathbf{C}$ are linear stiffness, mass and damping operators, respectively, $\boldsymbol{f}_{nl}$ is the nonlinear restoring force, $\boldsymbol{f}_E$ is the periodic external force, and $\mathbf{L}$ is a matrix of the linear boundary operator at the boundary coordinate $\boldsymbol{x}_B$, and may contain time derivatives. The vectors $\boldsymbol{q}, \boldsymbol{f}_{nl}$ and $\boldsymbol{f}_E$ are functions of position vector, $\boldsymbol{x}$, and time, t, which these arguments are dropped for convenience. The steady-state solution of Eq. (12) with the period of $T = 2\pi/\omega$ is obtained by expanding the deformation field based on the harmonic balance procedure:

$$\boldsymbol{q} = \sum_{j=0}^{n} (\boldsymbol{\psi}_j \cos(\omega_j t) + \boldsymbol{\varphi}_j \sin(\omega_j t)), \tag{13}$$

where $\boldsymbol{\psi}_j$ and $\boldsymbol{\varphi}_j$ are undetermined functions of the vibration amplitude at the frequency of $\omega_j = j\omega$. Recalling the same procedure and notations explained in Section 2.1, the continuous equations of motion are decoupled into one static ($j = 0$) and n dynamic ($j = 1, 2, \ldots, n$) equations as

$$(-\omega_j^2 \mathbf{M} - \imath\omega_j \mathbf{C} + \mathbf{K})\chi_j + \boldsymbol{f}_{nl_j} = \boldsymbol{f}_{E_j},$$
$$\mathbf{L}_j \chi_j = \mathbf{0} \quad \boldsymbol{x} \in \boldsymbol{x}_B. \tag{14}$$

For localized nonlinearities, the domain is partitioned into master and slave regions with respect to nonlinear forces,

$$\boldsymbol{f}_{nl} = \begin{cases} \boldsymbol{f}_{nl_\alpha} \neq \mathbf{0} & \boldsymbol{x} \in \boldsymbol{x}_\alpha \\ \mathbf{0} & \boldsymbol{x} \in \boldsymbol{x}_\beta \end{cases}. \tag{15}$$

Consequently, the field parameters and the equations of motion in Eq. (14) are separated into the following forms:

$$(-\omega_j^2 \mathbf{M} - \imath\omega_j \mathbf{C} + \mathbf{K})\chi_{\alpha_j} + \boldsymbol{f}_{nl_{\alpha_j}} = \boldsymbol{f}_{E_{\alpha_j}} \quad \boldsymbol{x} \in \boldsymbol{x}_\alpha,$$
$$\mathbf{L}_j \chi_j = \mathbf{0} \quad \boldsymbol{x} \in (\boldsymbol{x}_B \cap \boldsymbol{x}_\alpha), \tag{16}$$

and

$$(-\omega_j^2 \mathbf{M} - \imath\omega_j \mathbf{C} + \mathbf{K})\chi_{\beta_j} = \boldsymbol{f}_{E_{\beta_j}} \quad \boldsymbol{x} \in \boldsymbol{x}_\beta,$$
$$\mathbf{L}_j \chi_j = \mathbf{0} \quad \boldsymbol{x} \in (\boldsymbol{x}_B \cap \boldsymbol{x}_\beta). \tag{17}$$

In order to solve Eq. (16), additional information is required that can be obtained from the compatibility and continuity requirements on the interface between $\boldsymbol{x}_\alpha$ and $\boldsymbol{x}_\beta$ regions, named $\boldsymbol{x}_{\alpha\beta}$. Here Eq. (17) is used for constructing a linear relation that relates the internal forces at $\boldsymbol{x}_{\alpha\beta}$ to the external forces and deformations at $\boldsymbol{x}_{\alpha\beta}$,

$$\boldsymbol{f}_{I_{\beta_j}} = \mathbf{D}\chi_{\beta_j} = \mathbf{K}_{M_j}\chi_{\beta_j} + \boldsymbol{f}_{ET_{\beta_j}} \quad \boldsymbol{x} \in \boldsymbol{x}_{\alpha\beta}, \tag{18}$$

where $\boldsymbol{f}_{I_{\beta_j}}$ is the internal force, $\mathbf{D}$ is the differential operator transforming deformation field χ_{β_j} to internal force, $\mathbf{K}_{M_j}$ is an equivalent stiffness and $\boldsymbol{f}_{ET_{\beta_j}}$ is the projection of external forces (i.e., $\boldsymbol{f}_{E_{\beta_j}}$) on the interface, $\boldsymbol{x}_{\alpha\beta}$. Due to continuity of the

deformation and the internal forces at $\boldsymbol{x}_{\alpha\beta}$,

$$
\begin{aligned}
\boldsymbol{f}_{I_{\beta_j}} &= -\boldsymbol{f}_{I_{\alpha_j}} \\
\chi_{\beta_j} &= \chi_{\alpha_j}
\end{aligned}
\qquad \boldsymbol{x} \in \boldsymbol{x}_{\alpha\beta} .
\tag{19}
$$

Subsequently, the linear relation in Eq. (18) is imposed as a boundary condition on Eq. (16) and leads to

$$
(-\omega_j^2 \mathbf{M} - \imath\omega_j \mathbf{C} + \mathbf{K})\chi_{\alpha_j} + \boldsymbol{f}_{nl_{\alpha_j}} = \boldsymbol{f}_{E_{\alpha_j}} - \boldsymbol{f}_{ET_{\beta_j}} \quad \boldsymbol{x} \in \boldsymbol{x}_{\alpha},
$$

$$
\mathbf{L}_j \chi_j = \mathbf{0} \quad \boldsymbol{x} \in (\boldsymbol{x}_B \cap \boldsymbol{x}_{\alpha}),
$$

$$
(\mathbf{D} - \mathbf{K}_{M_j})\chi_{\alpha_j} = \mathbf{0} \quad \boldsymbol{x} \in \boldsymbol{x}_{\alpha\beta},
\tag{20}
$$

where $\boldsymbol{f}_{ET_{\beta_j}}$ is modeled as an external force applied to the border $\boldsymbol{x}_{\alpha\beta}$. Again, in order to find an appropriate orthogonal basis for χ_{α_j}, $\mathbf{K}_{M_j}$ and $\mathbf{L}_j$ are evaluated at the frequency ω_j so,

$$
(-\lambda_{jk}^2 \mathbf{M} - \imath\lambda_{jk} \mathbf{C} + \mathbf{K})\boldsymbol{\phi}_{jk} = \mathbf{0} \quad \boldsymbol{x} \in \boldsymbol{x}_{\alpha},
$$

$$
\mathbf{L}_j \boldsymbol{\phi}_{jk} = \mathbf{0} \quad \boldsymbol{x} \in (\boldsymbol{x}_B \cap \boldsymbol{x}_{\alpha}),
$$

$$
(\mathbf{D} - \mathbf{K}_{M_j})\boldsymbol{\phi}_{jk} = \mathbf{0} \quad \boldsymbol{x} \in \boldsymbol{x}_{\alpha\beta},
\tag{21}
$$

is the eigenvalue problem of the linearized condensed system, and $\boldsymbol{\phi}_{jk}$ is the kth eigenfunction vector and λ_{jk} is its companion eigenvalue. Therefore, χ_{α_j} can be approximated by a few mode shapes of the condensed system in the form of Eq. (9) (i.e., $\chi_{\alpha_j} \cong \boldsymbol{\Phi}_j(\boldsymbol{\eta}_{c_j} + \boldsymbol{\eta}_{s_j})$). Substituting Eq. (9) in Eq. (20) and using Galerkin method, the equations of motion are rewritten in the algebraic form of

$$
\boldsymbol{\Theta}_j(\boldsymbol{\eta}_{c_j} + \imath\boldsymbol{\eta}_{s_j}) + \langle \boldsymbol{f}_{nl_{\alpha_j}}, \boldsymbol{\Phi}_j \rangle = \langle \boldsymbol{f}_{E_{\alpha_j}} - \boldsymbol{f}_{ET_{\beta_j}}, \boldsymbol{\Phi}_j \rangle,
\tag{22}
$$

where

$$
\boldsymbol{\Theta}_j = \langle (-\omega_j^2 \mathbf{M} - \imath\omega_j \mathbf{C} + \mathbf{K})\boldsymbol{\Phi}_j, \boldsymbol{\Phi}_j \rangle.
$$

The real and imaginary parts of Eq. (22) result in two different nonlinear equations,

$$
\begin{bmatrix} \mathrm{Re}(\boldsymbol{\Theta}_j) & -\mathrm{Im}(\boldsymbol{\Theta}_j) \\ \mathrm{Im}(\boldsymbol{\Theta}_j) & \mathrm{Re}(\boldsymbol{\Theta}_j) \end{bmatrix} \begin{Bmatrix} \boldsymbol{\eta}_{c_j} \\ \boldsymbol{\eta}_{s_j} \end{Bmatrix} + \begin{Bmatrix} \mathrm{Re}(\langle \boldsymbol{f}_{nl_{\alpha_j}}, \boldsymbol{\Phi}_j \rangle) \\ \mathrm{Im}(\langle \boldsymbol{f}_{nl_{\alpha_j}}, \boldsymbol{\Phi}_j \rangle) \end{Bmatrix} = \begin{Bmatrix} \mathrm{Re}(\langle \boldsymbol{f}_{E_{\alpha_j}} - \boldsymbol{f}_{ET_{\beta_j}}, \boldsymbol{\Phi}_j \rangle) \\ \mathrm{Im}(\langle \boldsymbol{f}_{E_{\alpha_j}} - \boldsymbol{f}_{ET_{\beta_j}}, \boldsymbol{\Phi}_j \rangle) \end{Bmatrix} .
\tag{23}
$$

The final solution of the equations of motion is achieved by solving Eq. (23).

3. Numerical results and discussion

In what follows, to demonstrate the capabilities of the proposed reduction technique, discrete and continuous nonlinear vibrating systems are modeled numerically with weak and essential nonlinearities, and the results are compared with benchmark solutions.

The steady-state responses of these systems under periodic excitation are determined by the numerical method, the HBM and the proposed method. The resultant nonlinear algebraic equations of the HBM and the suggested method are solved by Newton–Raphson algorithm. The computational cost of Newton–Raphson algorithm at each step is proportional to the squared number of equations.

In addition, an experimental setup is prepared, and the method is used in identification of its nonlinear parameters. In these studies, the suggested method is applied to the problems, including popular types of nonlinearity consisting of dry friction, cubic stiffness and vibro-impact.

3.1. Discrete system case study

A bar resting on a rigid base on one side is employed as the first case study (see Fig. 1). This is an example of a system with a frictional interface. Using the distributed Jenkins element, the non-dimensional equations of motion for this system
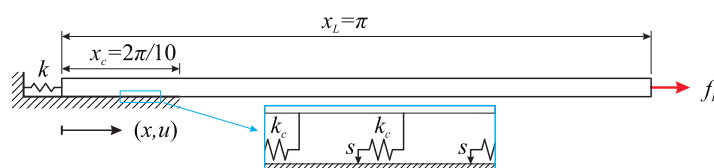

Fig. 1. A resting bar on a frictional support.

with Kelvin–Voigt internal damping are:

$$\frac{\partial^2 u}{\partial t^2} - \left(1 + c\frac{\partial}{\partial t}\right)\frac{\partial^2 u}{\partial x^2} + f_{nl} = f_E,$$

$$\left(1 + c\frac{\partial}{\partial t}\right)\frac{\partial u}{\partial x} = ku \quad x = 0,$$

$$\left(1 + c\frac{\partial}{\partial t}\right)\frac{\partial u}{\partial x} = 0 \quad x = x_L, \tag{24}$$

where

$$f_{nl} = k_c(u - s)(H(x) - H(x - x_c)),$$

$$f_E = F_E \delta(x - x_L)\cos(\omega t),$$

$$\frac{\partial s}{\partial t} = \begin{cases} 0 & |u - s| < \Delta_{stick} \\ \frac{\partial u}{\partial t} & |u - s| \geq \Delta_{stick} \end{cases},$$

and u is the axial displacement, $c = 1/50$ is the internal damping coefficient, $F_E = 1$ is the external force amplitude, $k = 1$ is a lumped stiffness at the left end of the bar, H is the unit step function and s, $k_c = 6$ and $\Delta_{stick} = 1$ are slip, stiffness and allowable stick displacement of the Jenkins elements, respectively.
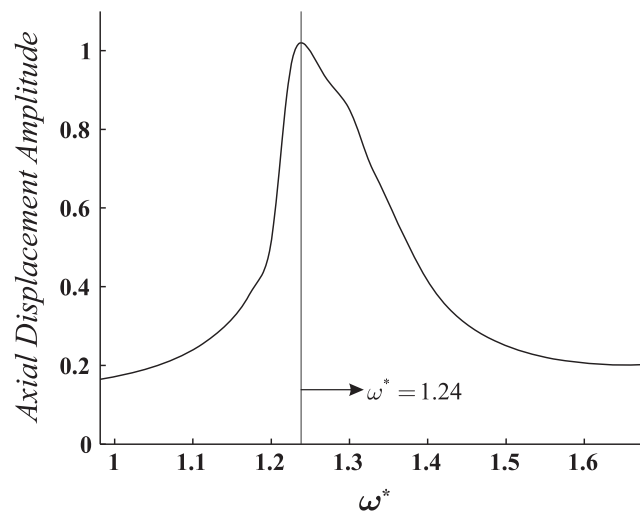

Fig. 2. The fundamental amplitude at $x = 0$ when the frequency is swept downward.
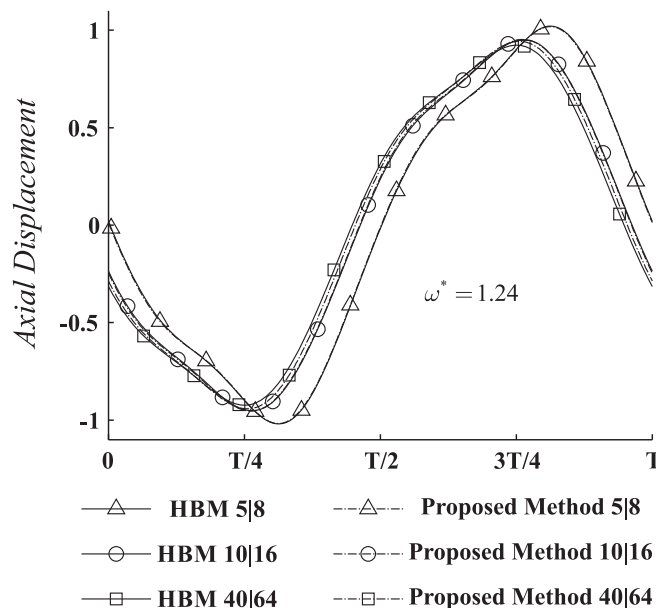

Fig. 3. The time responses of the bar at $x = 0$ for various mesh sizes at $\omega^* = 1.24$.

This system is discretized using the finite element method. The contact region and the rest of the domain are divided into 5 and 8 elements, respectively. The steady-state amplitude of the discretized system at the fundamental frequency for the node placed at $x = 0$ is shown in Fig. 2 (frequency is swept downward). The excitation frequency is normalized by the real part of the first natural frequency of the linearized system, $\omega_1 = 1.21$ (i.e., $\omega^* = \omega/\omega_1$).

The response of the system, truncated to order five (i.e., $n = 5$) at the resonance frequency $\omega^* = 1.24$, is shown in Fig. 3. In order to study the accuracy of results the mesh size is first refined to 10 and 16, then to 40 and 64 elements (labeled as 10| 16 and 40|64) for the contact and free region, respectively. In addition, the proposed method is applied to all three discretized systems using the first three mode shapes of the condensed system at the frequency $\omega^* = 1.24$. Only the resultant time response of the node placed at $x = 0$ is shown for summary and clarity in Fig. 3.

Fig. 3 reveals the three first mode shapes of the condensed systems are sufficient to predict the motion accurately. Using the proposed method, the computational cost is reduced by around 64 percent, 91 percent and 99.5 percent for 5|8, 10|16 and 40|64 mesh sizes compared with the HBM, respectively.

One can conclude the three first mode shapes of the condensed systems are sufficient to predict the deformation field of the nonlinear region for this case. The accuracy of the results depends on the discretization errors involved in estimating these mode shapes. In other words, using the mode shapes of a precisely condensed system leads to results that are more accurate. Therefore, it is expected that the reduction of a system based on the continuous method provides results that are more reliable.

3.2. Continuous system case studies

Case 1. The system shown in Fig. 1 with equations of motion (24) is condensed using the suggested method of continuous systems with the truncation order of five. Its first three mode shapes are used for reduction of the system at the frequency $\omega^* = 1.24$. The displacement at $x = 0$ is shown in Fig. 4.

From Fig. 4, one can observe the results of the proposed method applied to the continuous system are more accurate than those applied to the discretized system with 104 elements (40|64), while both systems are reduced with their first three mode shapes.

Case 2. The equations of motion of a cantilever beam (see Fig. 5) modeled with Timoshenko beam theory in a non-dimensional form are:

$$\mathbf{M}\ddot{\mathbf{q}} + \mathbf{C}\dot{\mathbf{q}} + \mathbf{K}\mathbf{q} + \mathbf{f}_{nl} = \mathbf{f}_E,$$

$$\mathbf{L}_i\mathbf{q} = \mathbf{0} \quad \mathbf{x} \in \mathbf{x}_{B_i}, \tag{25}$$

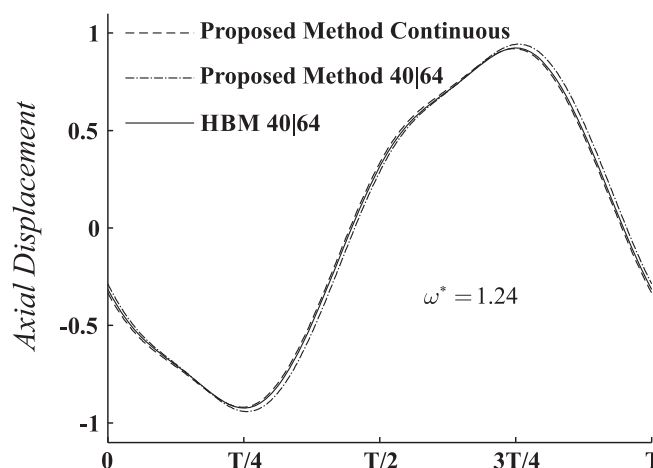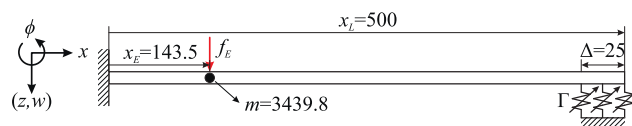**Fig. 4.** The time responses of the bar at $x = 0$.

Fig. 5. An elastic beam with localized nonlinearity of the cubic form.

where

$$\mathbf{M} = \begin{bmatrix} 1 & 0 \\ 0 & 1 + m\,\delta(x - x_E) \end{bmatrix}, \quad \mathbf{K} = \begin{bmatrix} -\frac{\partial^2}{\partial x^2} + \kappa & \kappa\frac{\partial}{\partial x} \\ -\kappa\frac{\partial}{\partial x} & -\kappa\frac{\partial^2}{\partial x^2} \end{bmatrix}, \quad \mathbf{C} = \begin{bmatrix} 0 & 0 \\ 0 & c_w \end{bmatrix},$$
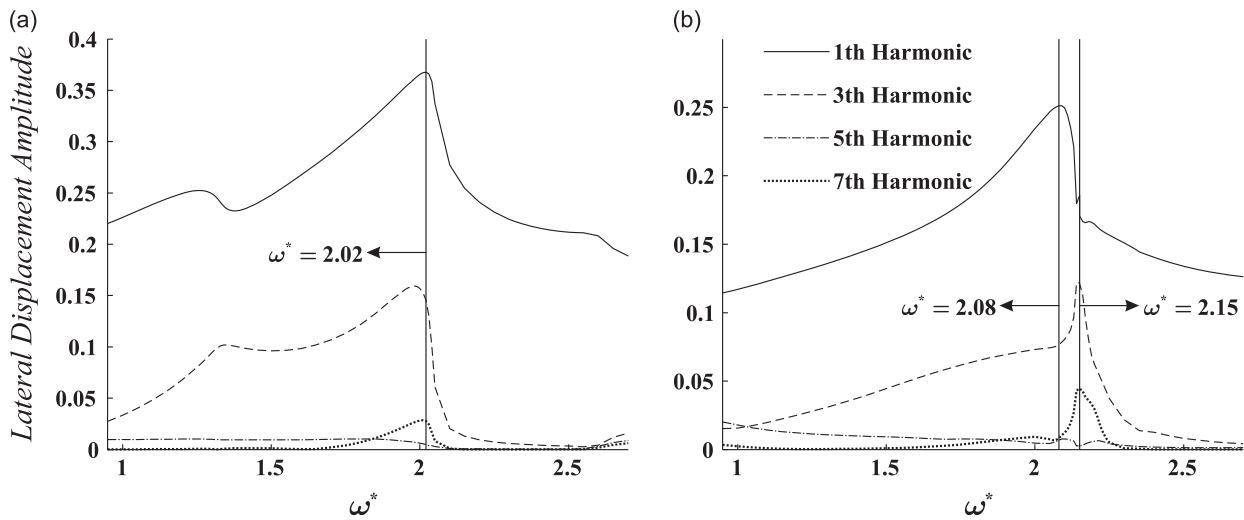

Fig. 6. The lateral displacement amplitudes of the beam free-end at each harmonic (a) weakly nonlinear system and (b) essentially nonlinear system.
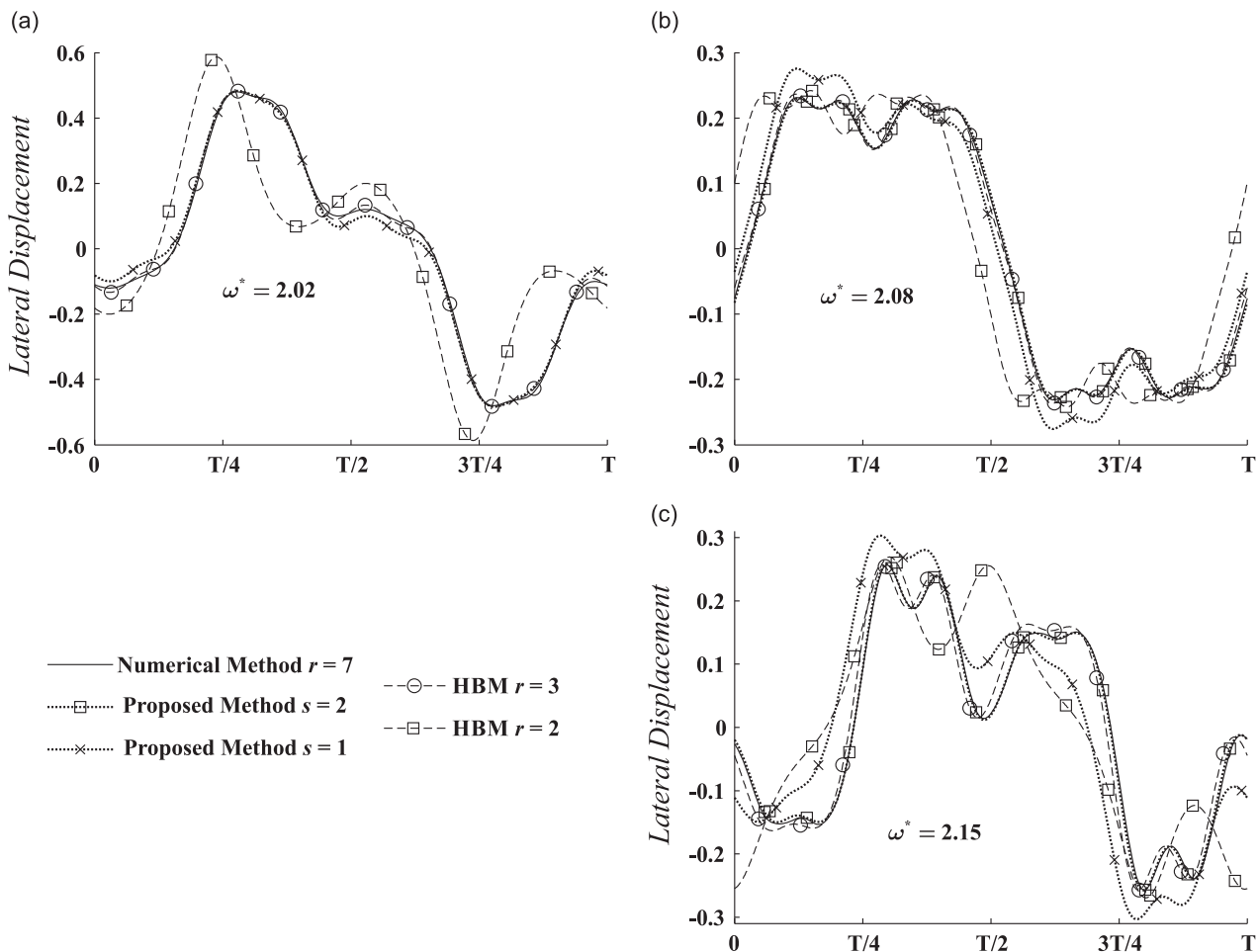

Fig. 7. The lateral displacements of the beam free-end at interested frequencies (a) weakly nonlinear system at $\omega^* = 2.02$, (b) essentially nonlinear system at $\omega^* = 2.08$ and (c) essentially nonlinear system at $\omega^* = 2.15$.

$$\boldsymbol{q} = \left\{ \begin{array}{c} \phi \\ w \end{array} \right\}, \quad \boldsymbol{f}_{nl} = \left\{ \begin{array}{c} 0 \\ \Gamma w^3 (H(x - (x_L - \Delta)) - H(x - x_L)) \end{array} \right\}, \quad \boldsymbol{f}_E = \left\{ \begin{array}{c} 0 \\ F_E \delta(x - x_E) \cos(\omega t) \end{array} \right\},$$

$$\mathbf{L}_1 = \begin{bmatrix} 1 & 0 \\ 0 & 1 \end{bmatrix} \quad x = 0, \quad \mathbf{L}_2 = \begin{bmatrix} \frac{\partial}{\partial x} & 0 \\ \kappa & \kappa \frac{\partial}{\partial x} \end{bmatrix} \quad x = x_L,$$
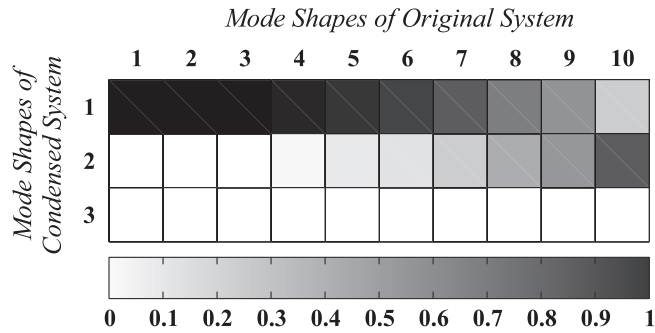

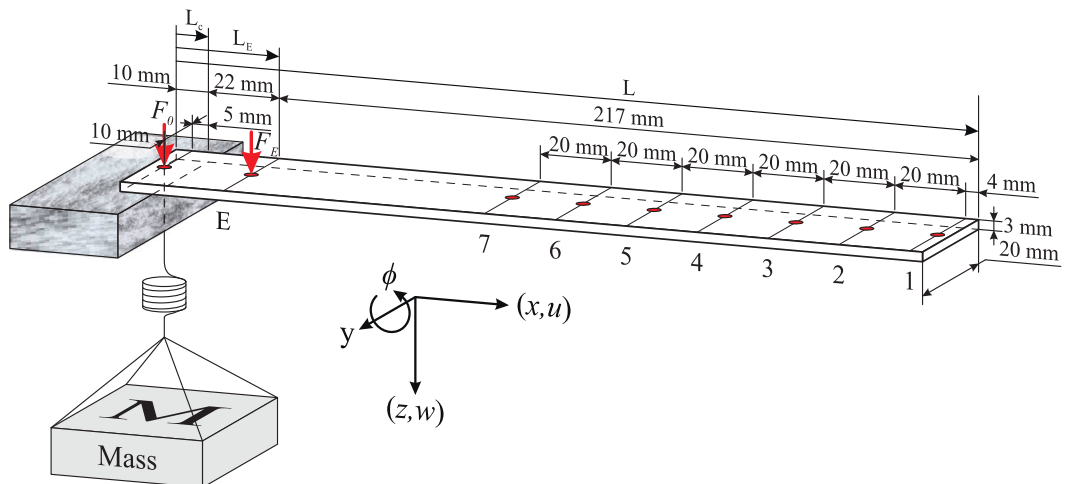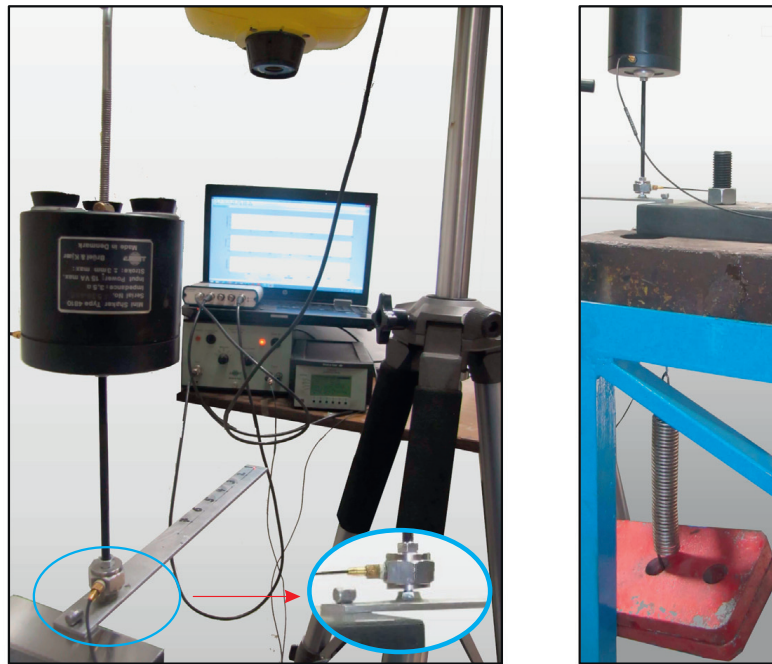Fig. 8. Plot of the MAC values between the mode shapes.

Fig. 9. The experimental test setup and dimensions.

and $\kappa = 0.331$, $c_w = 10^{-5}$, $F_E = 8 \times 10^{-8}$, δ and H are the Dirac delta and the unit step functions, respectively. m (mass of a lumped mass) and x_E are chosen such that the second resonance frequency is equal to three times that of the first resonance frequency. In the case of weak and essential nonlinearity, Γ shown in Fig. 5 is set to 15×10^{-7} and 100×10^{-7}, respectively.

The continuous system is discretized with the first r linearized undamped mode shapes of the system. Subsequently, the discretized system is solved by numerical and harmonic balance methods. The proposed method is also applied to the equations of motion with first s mode shapes of the condensed system, and the periodic responses are expanded to 11th harmonics. The amplitudes of each harmonic at the free end are shown in Fig. 6 around first resonance frequency. The real part of the first natural frequency of the linearized system, $\omega_1 = 6.97 \times 10^{-5}$, is used to normalize the excitation frequency (i.e., $\omega^* = \omega/\omega_1$).

As shown in Fig. 6a, a resonance occurs at $\omega^* = 2.02$ in the weakly nonlinear system. The response of the system at this frequency is shown in Fig. 7a at the free end. The predicted response of HBM with $r = 3$ is accurate, and when $r = 2$ the results become unacceptable. However, with $s = 1$, the proposed method can predict the response with an acceptable correlation. In comparison with the HBM, the proposed method reduces the computational cost by 90 percent.

The essentially nonlinear system is studied at two interested frequencies that are shown in Fig. 6b. The time responses of this system at these frequencies are shown in Fig. 7b and c at the free end. In these cases, the proposed method with $s = 1$ cannot predict the response with acceptable accuracy. Nevertheless, by increasing s, the results correlate with the other methods.

The mode shapes of the condensed system, used in expansion of deformation field, are linearly independent over the reduced domain. Therefore, the same number of these mode shapes covers more space than the mode shapes of the original system over the localized nonlinearity region. The degree of consistency over the reduced domain between these two sets of mode shapes for $j = 1$ is shown in Fig. 8 using the Modal Assurance Criteria (MAC).

From Fig. 8, one can conclude that the proposed method with two mode shapes (i.e., $s = 2$) and the HBM with 10 mode shapes (i.e., $r = 10$) lead to results with the same precision. In this example, the suggested method reduces 96 percent of computational cost compared with the HBM.

3.3. Experimental case study

The aluminum beam shown in Fig. 9, resting on a frictional support at one end and free on the other side, is employed as an experimental case study. A constant normal preload at the support is provided by suspended mass blocks. The dynamic response of the system becomes nonlinear when the motion amplitude is large enough to cause slip and vibro-impacts at the support.
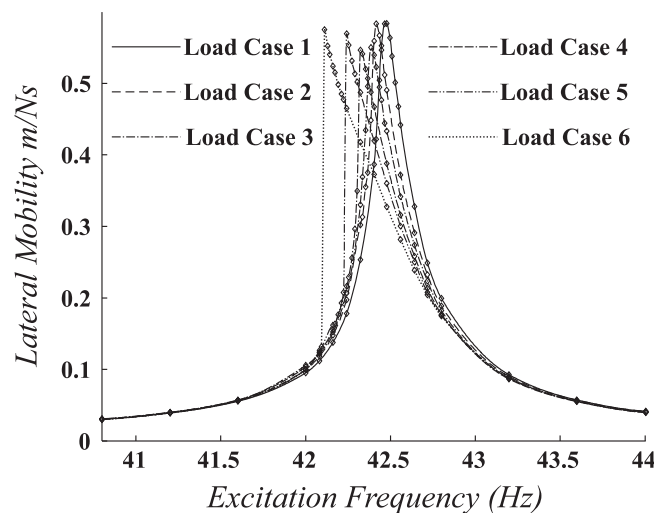

Fig. 10. The measured frequency responses for the six excitation levels, ◇ shows measured points.

Table 1
Resonance data extracted from experimental measurements.

Load case	1	2	3	4	5	6
Resonance frequency (Hz)	42.48	42.41	42.38	42.32	42.24	42.11
Force amplitude (mN)	121	170	198	217	246	278

The frequency responses of the system at six excitation levels are shown in Fig. 10. The results summarized in Table 1 are obtained by exiting the system at point E and measuring the response at point 7 (see Fig. 9). At each excitation level, a single harmonic force is applied to the beam at its resonance frequency. A laser Doppler is employed to record velocities of the system at points 1–7.

It is noted that the vibro-impacts and the slip at support excite even and odd higher harmonics, respectively. The dominant higher harmonics in the recorded data are all even harmonics, indicating the nonlinear phenomenon is due to the vibro-impacts. Furthermore, the internal resonance between the first and second modes of the beam ($\omega_2 = 6\omega_1$) causes the amplitude of 6th harmonics to be larger than other higher harmonics from the load case 4 onward.

Based on the observed behavior of the system the support reaction force is related to the beam deformation field by Hunt–Crossley model [13] in normal direction. The reaction forces in tangential direction are modeled as uniformly distributed stiffness, as no-slip motion was observed in the frictional support. The equations of motion of the system with the displacement field $\boldsymbol{q} = \{u, \phi, w\}^T$, representing axial, rotational and lateral motions, in a non-dimensional form are

$$(\mathbf{M}_1 + \delta(x - L_E)\mathbf{M}_2)\ddot{\boldsymbol{q}} + \mathbf{C}\dot{\boldsymbol{q}} + \mathbf{K}\boldsymbol{q} + \boldsymbol{f}_{nl} = \boldsymbol{f}_E + \boldsymbol{f}_{E_0},$$

$$\mathbf{L}\boldsymbol{q} = \mathbf{0} \quad \boldsymbol{x} \in \boldsymbol{x}_B. \tag{26}$$

The mass distribution of the beam is $\mathbf{M}_1$, and $\mathbf{M}_2$ introduces the mass effects of the force transducer. The stiffness damping and boundary condition operators of the system are defined as

$$\mathbf{K} = \begin{bmatrix} -\frac{\partial^2}{\partial x^2} & 0 & 0 \\ 0 & -\frac{\partial^2}{\partial x^2} + \kappa & +\kappa\frac{\partial}{\partial x} \\ 0 & -\kappa\frac{\partial}{\partial x} & -\kappa\frac{\partial^2}{\partial x^2} \end{bmatrix}, \quad \mathbf{C} = c\mathbf{K},$$

$$\mathbf{L} = \left(1 + \frac{\partial}{\partial t}c\right) \begin{bmatrix} \frac{\partial}{\partial x} & 0 & 0 \\ 0 & \frac{\partial}{\partial x} & 0 \\ 0 & \kappa & \kappa\frac{\partial}{\partial x} \end{bmatrix}, \quad x_B = 0, L. \tag{27}$$

Table 2
Comparison of dominant harmonics in identified model and recorded experimental data.

Load case	Harmonic number							
	1		2		4		6	
	a_R/a_S	$\Delta\theta°$	a_R/a_S	$\Delta\theta°$	a_R/a_S	$\Delta\theta°$	a_R/a_S	$\Delta\theta°$
1	1.003	−0.079	–	–	–	–	–	–
2	1.002	−0.014	–	–	–	–	–	–
3	1.002	0.032	–	–	–	–	–	–
4	1.006	0.950	–	–	–	–	0.947	0.724
5	1.007	0.129	1.001	0.846	0.920	−14.448	0.997	−0.834
6	1.013	0.225	1.001	0.342	0.962	−11.696	1.006	0.265
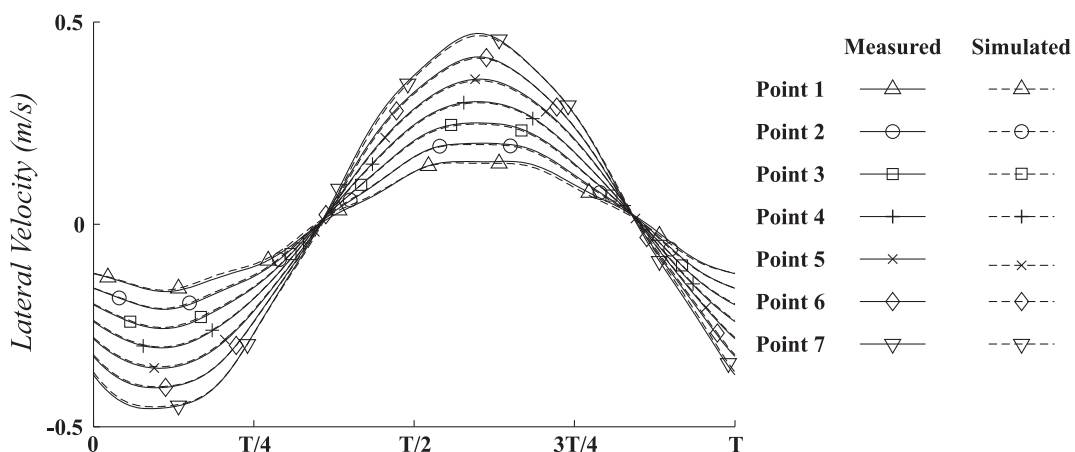
Fig. 11. The time responses of the experimental setup at the resonance frequency of the load case 6.

where $\kappa = 0.331$ is the shear correction factor of the beam section. The nonlinear restoring forces are

$$\boldsymbol{f}_{nl} = \boldsymbol{f}_c(H(x) - H(x - L_c)),$$

$$\boldsymbol{f}_c = \begin{cases} \left\{ k_T(u+\phi), 3k_T(u+\phi), k_N w\left(1 + \frac{c_e}{\dot{w}^{(-)}}\dot{w}\right) \right\}^T & w > 0 \\ \{0, 0, 0\}^T & w \leq 0 \end{cases}, \tag{28}$$

where k_T and k_N are the contact tangential and normal stiffness, c_e is a constant coefficient, all of which are unknown and are selected as design variables in this identification practice. $\dot{w}^{(-)}$ is the initial normal impact velocity. The external forces are also defined as

$$\boldsymbol{f}_E = \{0, 0, F_E \, \cos(\omega t)\}^T \delta(x - L_E),$$

$$\boldsymbol{f}_{E_0} = \{0, 0, F_0\}^T (H(x) - H(x - L_c)), \tag{29}$$

where F_E is the excitation force amplitude and F_0 is the constant contact preload.

Using the proposed method for the continuous systems, the beam model is condensed to the nonlinear domain at the excited frequencies, and its first eight mode shapes are utilized to reduce the system size.

The excitation force applied to the test structure was introduced to Eq. (26) and the unknown parameters of the contact are tuned to minimize the difference between the measured responses and the model predictions. In the identification procedure, initial values for the parameters are selected and the residues are minimized using a gradient-based optimization method. The identification procedure was repeated for a number of initial guesses to ensure the uniqueness of the identified parameters.

Unknown parameters of the contact model are identified, and the results of the analytical model are compared to the recorded experimental data in Table 2. In this table the ratios of the recorded harmonic, a_R, to the one obtained from the simulation, a_S, are tabulated. It is seen that these ratios in the dominant harmonics of the response are close to unity. Also, in this table the phase difference, $\Delta\theta^\circ$, between the measured and the simulated responses of the dominant harmonics is tabulated. It is seen that in all harmonics except for the fourth harmonic, the phase difference is less than 1°. The maximum errors are observed in the fourth harmonic with 8 percent error in the amplitudes, and 14° phase difference.

The correlation between the recorded velocity and those obtained from the identified model for the load case 6 is shown in Fig. 11. Excellent agreements between the two sets of measured and model predictions are achieved. It indicates that the condensed model captures all the dominant effects of the original system, and it was successfully used for identification of the contact parameters.

4. Conclusions

This paper proposed a condensation technique for solving nonlinear systems with localized nonlinearities under periodic motion. The systems equations of motion are reduced to regions of the localized nonlinearities. A few mode shapes of the linearized reduced system are utilized as a basis to expand deformations of the localized nonlinearities in each harmonic. These mode shapes are linearly independent, and their wavelengths are confined to the size of the reduced domain. The condensation process converts the system equations of motion to a small set of nonlinear algebraic equations in each harmonic.

Accuracy and computational cost of the method were discussed in various numerical studies, and were compared with the HBM. Furthermore, this reduction approach was successfully used in identification of a system whose response was measured in an experimental setup. The outcomes of these studies show potentials of the proposed method in reduction of computational cost, while preserving the accuracy, identification and health monitoring of the systems conducted within the scope of this paper. The reduction method can also be applied to the nonlinear systems along with other solution methods such as AHBM and IHB and easily implemented in FEM codes.

References

[1] Z. Qu, *Model Order Reduction Techniques: With Applications in Finite Element Analysis*, First Edition, Springer-Verlag, London, 2004.

[2] G. Kerschen, M. Peeters, J.C. Golinval, A.F. Vakakis, Nonlinear normal modes, Part I: a useful framework for the structural dynamicist, *Mechanical Systems and Signal Processing* 23 (2009) 170–194.

[3] M. Peeters, R Viguie, G Serandour, G Kerschen, J Golinval, Nonlinear normal modes, Part II: toward a practical computation using numerical continuation techniques, *Mechanical Systems and Signal Processing* 23 (2009) 195–216.

[4] D. Jiang, C. Pierre, S. Shaw, The construction of non-linear normal modes for systems with internal resonance, *International Journal of Non-Linear Mechanics* 40 (2005) 729–746.

[5] D. Jiang, C. Pierre, C., S. Shaw, Nonlinear normal modes for vibratory systems under harmonic excitation, Journal of Sound and Vibration, 288 (2005) 791–812.

[6] M. Legrand, D. Jiang, C. Pierre, S. Shaw, Nonlinear normal modes of a rotating shaft based on the invariant manifold method, *International Journal of Rotating Machinery* 10 (2004) 319–335.

[7] E. Butcher, Clearance effects on bilinear normal mode frequencies, *Journal of Sound and Vibration* 224 (1999) 305–328.

[8] T.A. Doughty, P. Davies, A.K. Bajaj, A comparison of three techniques using steady state data to identify non-linear modal behavior of an externally excited cantilever beam, *Journal of Sound and Vibration* 249 (2002) 785–813.

[9] S.L. Lau, Y.K. Cheung, Amplitude incremental variational principle for nonlinear vibration of elastic systems, *Journal of Applied Mechanics* 48 (1981) 959–964.
[10] A. Grolet, F. Thouverez, On a new harmonic selection technique for harmonic balance method, *Mechanical Systems and Signal Processing* 30 (2012) 43–60.
[11] Y. Kim, S. Noah, Response and bifurcation analysis of a MDOF rotor system with a strong nonlinearity, *Nonlinear Dynamics* 2 (1991) 215–234.
[12] Y. Kim, S. Noah, Stability and bifurcation analysis of oscillators with piecewise-linear characteristics: a general approach, *Journal of Applied Mechanics* 58 (1991) 545–553.
[13] K. Hunt, F. Crossley, Coefficient of restitution interpreted as damping in vibroimpact, *Journal of Applied Mechanics* 42 (1975) 440.